AIP | Journal of Applied Physics

Laser-induced breakdown spectroscopy of trisilane using infrared CO2 laser pulses

J. J. Camacho, J. M. Poyato, L. Díaz, and M. Santos

Citation: J. Appl. Phys. 102, 103302 (2007); doi: 10.1063/1.2811870
View online: http://dx.doi.org/10.1063/1.2811870
View Table of Contents: http://jap.aip.org/resource/1/JAPIAU/v102/i10
Published by the American Institute of Physics.

Related Articles

Photoluminescence properties of (Ce3+, Mn2+)-codoped CaCO3 red phosphor
J. Appl. Phys. 113, 033519 (2013)

Synthesis and photoluminescence of fluorinated graphene quantum dots
Appl. Phys. Lett. 102, 013111 (2013)

The luminescence characteristics of CsI(Na) crystal under α and X/γ excitation
J. Appl. Phys. 113, 023101 (2013)

Structural and optoelectronic properties of Eu2+-doped nanoscale barium titanates of pseudo-cubic form
J. Appl. Phys. 112, 124321 (2012)

Quantum yield of luminescence of Ag nanoclusters dispersed within transparent bulk glass vs. glass composition and temperature
Appl. Phys. Lett. 101, 251106 (2012)

Additional information on J. Appl. Phys.

Journal Homepage: http://jap.aip.org/
Journal Information: http://jap.aip.org/about/about_the_journal
Top downloads: http://jap.aip.org/features/most_downloaded
Information for Authors: http://jap.aip.org/authors

ADVERTISEMENT

Downloaded 22 Jan 2013 to 161.111.22.141. Redistribution subject to AIP license or copyright; see http://jap.aip.org/about/rights_and_permissions

Laser-induced breakdown spectroscopy of trisilane using infrared CO_2 laser pulses

J. J. Camacho[a)] and J. M. L. Poyato
Departamento de Química-Física Aplicada, Facultad de Ciencias, Universidad Autónoma de Madrid, Cantoblanco, 28049 Madrid, Spain

L. Díaz and M. Santos
Instituto de Estructura de la Materia, CFMAC, CSIC, Serrano 121, 28006 Madrid, Spain

(Received 14 May 2007; accepted 19 September 2007; published online 20 November 2007)

The plasma produced in trisilane (Si_3H_8) at room temperature and pressures ranging from 50 to 10^3 Pa by laser-induced breakdown (LIB) has been investigated. The ultraviolet-visible-near infrared emission generated by high-power IR CO_2 laser pulses in Si_3H_8 has been studied by means of optical emission spectroscopy. Optical breakdown threshold intensities in trisilane at 10.591 μm for laser pulse lengths of 100 ns have been measured as a function of gas pressure. The strong emission observed in the plasma region is mainly due to electronic relaxation of excited atomic H and Si and ionic fragments Si^+, Si^{2+}, and Si^{3+}. An excitation temperature $T_{exc}=5600\pm300$ K was calculated by means of H atomic lines assuming local thermodynamic equilibrium. The physical processes leading to LIB of trisilane in the power density range $0.28\ \mathrm{GW\,cm^{-2}} < J < 3.99\ \mathrm{GW\,cm^{-2}}$ have been analyzed. From our experimental observations we can propose that, although the first electrons must appear via multiphoton ionization, electron cascade is the main mechanism responsible for the breakdown in trisilane. © *2007 American Institute of Physics*. [DOI: 10.1063/1.2811870]

I. INTRODUCTION

Laser-induced breakdown (LIB) also called laser-induced dielectric breakdown (LIDB) is the partial or complete ionization of a sample through absorption of laser radiation. The ionization produces a plasma which is more effective in absorbing the optical radiation than ordinary matter. Optical breakdown occurs primarily for short pulses where the short interaction times do not allow thermal breakdown.[1] In this case, the high peak powers and irradiances of short laser pulses produce the plasma through electron cascade ionization or inverse bremsstrahlung and direct ionization by multiphoton absorption. The latter process involves simultaneous absorption of a certain number of photons by an atom or molecules to cause its ionization. This mechanism produces a number of initial free electrons in the focal volume and, although it is not the major process in the growth of electrons in the laser plasma, it is more important for short wavelength laser ($\lambda < 1$ μm) or low pressure ($P < 1300$ Pa).[2] In the former process of electron cascade ionization, the free electrons in the focal volume are accelerated by the electric field of the laser by gaining energy. After the electrons have sufficient energy, they can ionize different species (atoms, molecules, and ions) by collision making the electron density grow exponentially with time. This process is more important for long wavelength laser ($\lambda > 1$ μm) and high pressure ($P > 13\,000$ Pa).[2] The plasma is thus rapidly heated by the laser beam to very high temperatures, producing plasma expansion, an audible acoustic signature, and a visible plasma emission.

The knowledge about the properties of mono-, di-, and trisilanes has become greatly important because of their wide practical use in the semiconductor industry. LIB methods are important for a more complete understanding of the photo-induced chemical vapor processes to produce thin nanostructured films of hydrogenated amorphous silicon (a-Si:H). These processing technologies generally imply deposition of a film on a substrate as, for example, in experiments with magnetron sputtering,[3] plasma deposition,[4] laser ablation,[5–7] and electric spark processing of a silicon wafer.[8] LIB of silane (SiH_4) has been largely used in laser-induced chemical vapor deposition (CVD) and plasma-enhanced CVD for obtaining amorphous and hydrogenated silicon films.[9–15] Besides, higher silanes (disilane and trisilane), more effective in absorbing IR radiation, have been described as very suitable to act as precursors to a-Si:H films and from plasma decomposition induced by glow discharge. A major feature of these processes is a deposition rate enhancement of a factor of over 20 compared to monosilane.[16]

Laser-induced breakdown spectroscopy (LIBS) is becoming one of the most promising tools for rapid spectrochemical analysis of solid, liquid, or gas. Detailed reviews on the LIBS principle and applications can be found in Refs. 17–22. The ultraviolet-visible-near infrared (UV-Vis-NIR) spectral region investigated by LIBS largely elucidates the elemental composition of the laser target by profiling the atomic spectral emission lines; limited information on molecular species, however, may be derived. Measurements of the UV-Vis-NIR spectra revealed highly ionized plasma which expanded like a blast wave into the surrounding environment. Laser produced plasmas offer the advantages of detecting low impurity concentration, high repetition rate,

a)Author to whom correspondence should be addressed. Electronic mail: j.j.camacho@uam.es

0021-8979/2007/102(10)/103302/10/$23.00 © 2007 American Institute of Physics

Downloaded 22 Jan 2013 to 161.111.22.141. Redistribution subject to AIP license or copyright; see http://jap.aip.org/about/rights_and_permissions

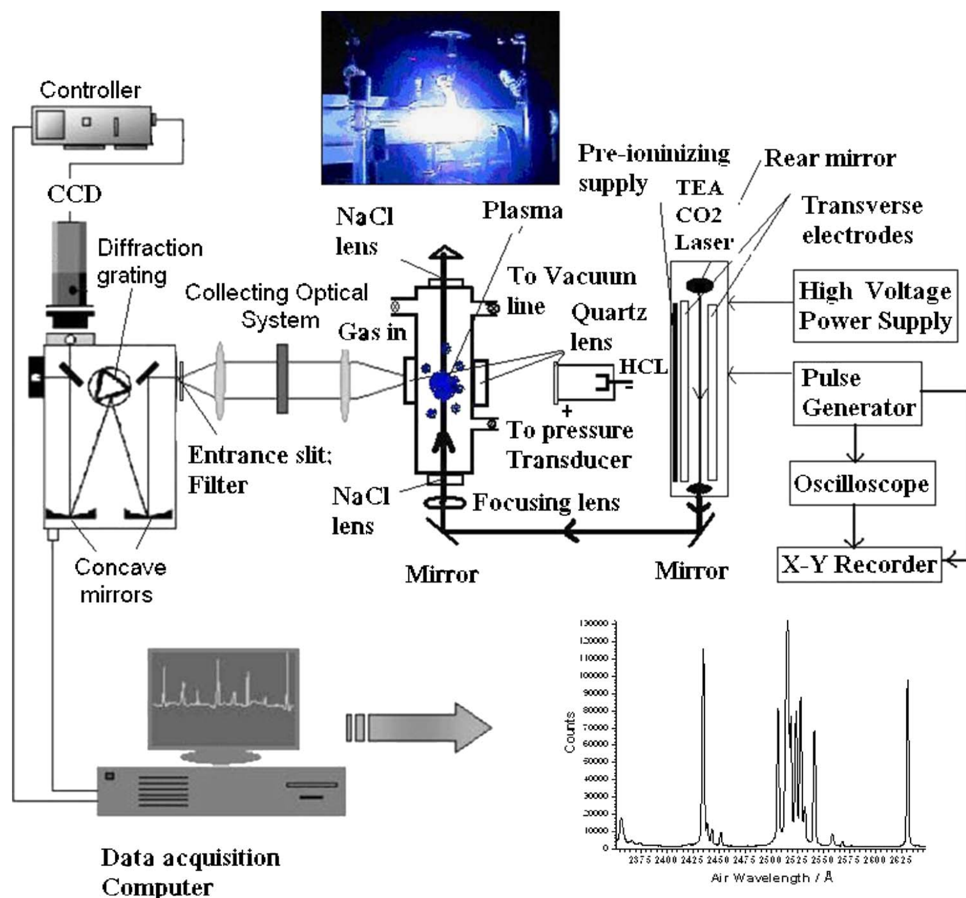

FIG. 1. (Color online) Schematic diagram of the experimental setup for laser-induced breakdown diagnostics.

stability, the absence of electrical noise, and scalability to high densities where collision rates are high. This will help to produce quickly a local thermodinamical equilibrium (LTE). In spite of the great deal of work that has been done recently, the understanding of the development of the plasma for laser energies and gas pressures close to the threshold appears to be incomplete. Particularly for trisilane, there is a notable lack of information on the plasma conditions just after breakdown, the spatial distribution and its change with time.

The experiments which are reported here describe the appearance of the plasma during its radiative phase. Optical emission spectroscopy (OES) has been used to investigate the chemical consequences of breakdown in trisilane. Optical breakdown threshold intensities in Si_3H_8 have been determined for different pressures. The emission observed in the plasma is mainly due to electronic relaxation of excited atomic H and Si and ionic fragments Si^+, Si^{2+}, and Si^{3+}. The excitation temperature and electron density were obtained from atomic H lines. The physical processes leading to LIB of trisilane have been analyzed.

II. EXPERIMENTAL DETAILS

The experimental configuration used to study trisilane by LIBS is shown in Fig. 1. Also, at the top of the Fig. 1, we show an image of LIB trisilane plasma. The light source used was a Lumonics model K-103 transverse excitation atmospheric CO_2 laser operating on an 8:8:84 mixture of CO_2:N_2:He, respectively. The laser is equipped with a frontal Ge multimode optics (35% reflectivity) and a rear diffraction grating with 135 lines/mm blazed at 10.6 μm. The CO_2 laser irradiation of trisilane was carried out using the 10P(20) line at 10.591 μm. This wavelength, absorbed by trisilane, was checked with a 16-A spectrum analyzer (Optical Eng. Co.). The pulse temporal profile was monitored with a photon drag detector (Rofin Sinar 7415). The pulse consisted of a spike [100 ns—full width at half maximum (FWHM)] and a tail lasting approximately 3 μs. The optical breakdown was produced in a pyrex cell of 4.5 cm diameter and 43 cm length equipped with two NaCl windows for the IR laser beam orthogonal to two quartz windows for optical detection. Focused geometry was used by placing a NaCl lens (24 cm focal length) in front of the cell for the CO_2 laser beam. The CO_2 laser fluence was calculated as the ratio of the pulse energy (measured in front of the lens with a Lumonics 20D pyroelectric detector through a Tektronix TDS 540 digital oscilloscope) and the 1/e cross-sectional beam area (measured at the cell position with a pyroelectric array Delta Development Mark IV). In our experimental conditions, a laser power density of 0.86 ± 0.01 GW cm^{-2} was used. Between two measurements series, the vacuum chamber was evacuated with a rotary pump to a residual of 5 Pa. Before every experiment, the cell was disassembled, cleaned, and filled with trisilane at a pressure ranging from 50 ± 5 to 1000 ± 5 Pa that was measured by a mechanical gauge. Trisilane was kindly supplied by Prof. R. Becerra (purity better than 96%). The filled cell was then closed and transported to the laser facility. The plasma radiation was

Downloaded 22 Jan 2013 to 161.111.22.141. Redistribution subject to AIP license or copyright; see http://jap.aip.org/about/rights_and_permissions

imaged by a collecting optical system onto the entrance slit of different monochromators. Two spectrometers were used: ISA Jobin Yvon Spex (Model HR320) 0.32 m equipped with a plane holographic grating (2400 grooves/mm) in the spectral region of 2000–7500 Å at a resolution of ~0.12 Å in first order; and a 1/8 m Oriel spectrometer (10 and 25 μm slits) with two different gratings (1200 and 2400 grooves/mm) in the spectral region of 2000–11000 Å at a resolution of ~1.3 Å in first order (1200 grooves/mm grating). The detector was an Andor DU420-OE (open electrode) charge-coupled device (CCD) camera (1024×256 matrix of 26×26 μm^2 individual pixels) with thermoelectric cooling working at −30 °C. The intensity response of the detection system was calibrated with a standard (Osram No. 6438, 6.6 A, 200 W) halogen lamp[23] and a Hg/Ar pencil lamp.[24] Several (Cu/Ne, Fe/Ne, and Cr/Ar) hollow cathode lamps (HCLs) were used for the spectral wavelength calibration of the spectrometers

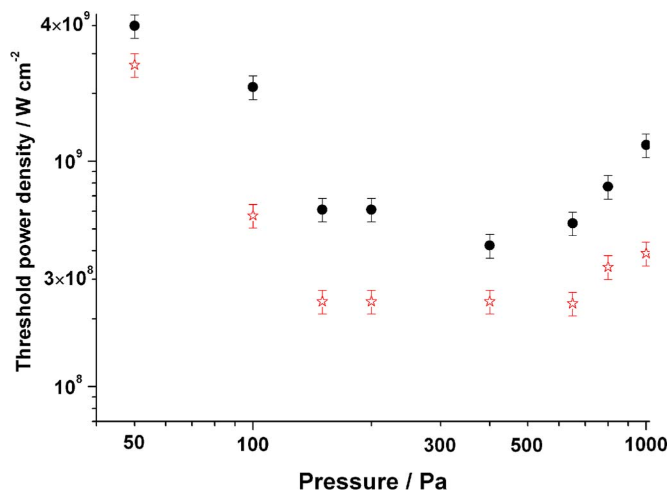

FIG. 2. (Color online) Threshold power density of optical breakdown in trisilane for different pressures. Solid circle: without previous breakdown; open star: with previous breakdown.

III. RESULTS AND DISCUSSION

A. Optical breakdown threshold intensities for Si_3H_8

The minimum power density required to form a plasma is called the breakdown threshold; different types of laser, sample, and environmental conditions will have different breakdown thresholds. Breakdown thresholds of solids and liquids are usually much lower than those for gases. Several models have been proposed to describe the LIDB.[25–29] From these models the breakdown induced by IR laser seems to be quite well explained as a collisional assisted avalanche ionization mechanism in which the development of the gas breakdown is determined by the presence of some free electron in the focal volume. It is deduced from the cited models that the procedure to do the measurements of the threshold power density determines the measured value. Some authors induce the breakdown at a pressure over the desired value, later the pressure is lowered, and the energy adjusted until the breakdown begins with some probability, usually around 50%.[25] This method is similar to inducing the breakdown with energy in excess and to attenuating the laser until the spark disappears.[30] In these cases it could be that initial free electrons have been produced by previous breakdowns and they are the seed of the avalanche process.[27] Another way to induce the breakdown is to fix the pressure and to gradually increase the energy until a visible spark is observed around the focal region in a determined number of laser pulses, again 50%.[31] In this last method the obtained threshold value is increased by more than 25% in respect to the previous one.[32] Both methods have been used to measure the trisilane breakdown at different pressures and the results are shown in Fig. 2. As can be seen, the behavior of both curves is similar. In the case of trisilane, we have found that the range of threshold power density is lower than for noble or nitrogen gases[33] by at least one order of magnitude. This fact can be due to the formation of solid silicon, which favors the breakdown process. The lower intensities that have been obtained for the breakdown threshold (see Fig. 2) could be also related to the used focal length (24 cm) and beam size in the focal region (7.85×10^{-3} cm^2), favoring the decrease of the intensity due to the lack of the diffusion losses.

B. Identification of the chemical species in the laser-induced trisilane plasma

In the scanned spectral region, from ultraviolet to near infrared, the optical spectra show a peculiar LIB emission. Characteristics of optical emission spectra change in time and in space. In particular, in the proximity of the plasma plume and at the beginning of the plasma expansion, the emission spectra are dominated by a continuum emission. This continuum is due to the interactions between free electrons (bremsstrahlung) and to the interaction of free and bound electrons (recombination continuum). The former ones are particularly important in the UV spectral region, whereas the latter ones are important at longer wavelengths. In general, the emission spectra at higher distances from the plasma plume are mainly characterized by atoms and ions, but only few molecular species. In fact the plasma is strongly ionized in such experimental conditions. Some authors have reported molecular emission due to SiH and Si_2 in plasma-induced by lasers.[10,34,35] On the other hand, Nozaki *et al.*[36] have detected SiH_3 in a H_2/SiH_4 system and have shown that SiH_3 is one of the strongest candidates for the film precursor in the catalytic CVD. Although this species can exist under certain conditions in plasmas, we do not observe emission due to electronically excited molecular species.

Optical LIB emission spectra of trisilane (Figs. 3–7) were acquired in the 2000–8790 Å region at a pressure of 650 Pa. Figs. 3–7 display such spectra and the assignment of the atomic lines of H, Si, Si^+, Si^{2+}, and Si^{3+} tabulated in NIST Atomic Spectral Database.[37–47] In the spectrum of Fig. 3 in the 2000–3460 Å region, not only strong atomic Si lines dominate, but also weak Si^+ and Si^{2+} lines are observed. In this spectrum the predominant emitting species are the Si $3s^23p^2\,{}^1D_2 \leftarrow 3s^23p4s\,{}^1P^0_1$ atomic line at 2881.579 Å, Si $3s^23p^2\,{}^1D_2 \leftarrow 3s^23p4s\,{}^3P^0_1$ atomic line at 2987.645 Å and the multiplet structure of Si $3s^23p^2\,{}^3P_{J''} \leftarrow 3s^23p4s\,{}^3P^0_{J'}$ around

Downloaded 22 Jan 2013 to 161.111.22.141. Redistribution subject to AIP license or copyright; see http://jap.aip.org/about/rights_and_permissions

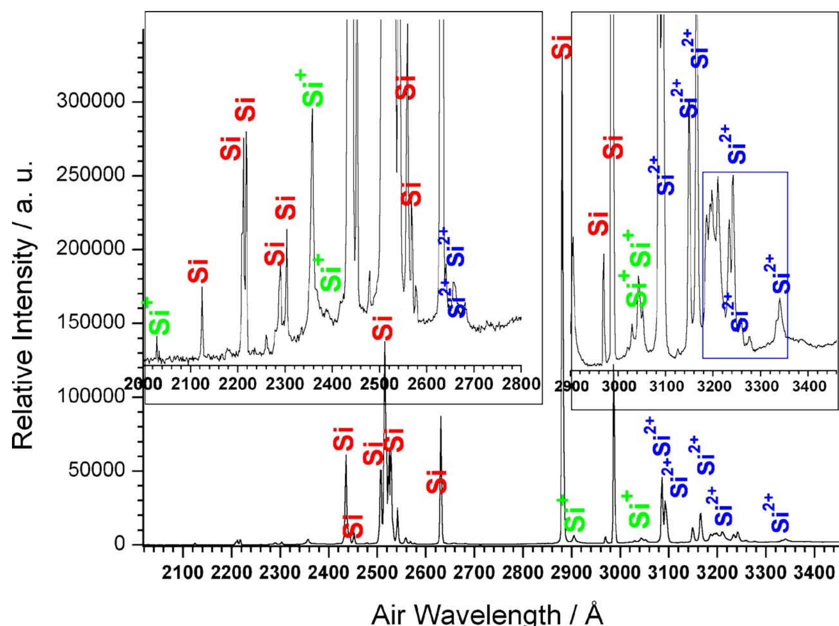

FIG. 3. (Color online) Low-resolution LIB emission spectrum observed in the 2000–3460 Å region in trisilane gas at a pressure of 650 Pa, excited by the 10P(20) line at 944.20 cm^{-1} of the CO_2 laser, and assignment of the atomic lines of Si, Si^+, and Si^{2+}.

2516 Å. Several lines of Si^{2+} around 3086 Å are due to the multiplet transition $3s3d\ ^3D_{J''} \leftarrow 3s4p\ ^3P^0_{J'}$. In the LIB emission spectrum observed in the 3400–4910 Å region (Fig. 4), the predominant emitting species are the Si $3s^23p4s\ ^1P^0_1 \rightarrow 3s3p^2\ ^1S_0$ atomic line at 3905.523 Å, the Si^+ $3s^23d\ ^2D_{5/2} \leftarrow 3s^24f\ ^2F^0_{7/2}$ line at 4130.89 Å, and the second line of the Balmer series H_β $n=2 \leftarrow n=4$ at 4861.33 Å. In the spectrum of Fig. 4, many ionized lines of Si^{2+} and Si^{3+}, and many lines of the Balmer series of hydrogen are also present. In the LIB emission spectrum observed in the 4920–6320 Å region (Fig. 5), the predominant emitting species are the Si^+ $3s^24p\ ^2P^0_{1/2} \leftarrow 3s^24d\ ^2D_{3/2}$ atomic line at 5041.03 Å, Si^+ $3s^24p\ ^2P^0_{3/2} \leftarrow 3s^24d\ ^2D_{5/2}$ atomic line at 5055.98 Å, Si^+ $3s^24p\ ^2P^0_{1/2} \leftarrow 3s^25s\ ^2S_{1/2}$ atomic line at 5957.56 Å and the Si^+ $3s^24p\ ^2P^0_{3/2} \leftarrow 3s^25s\ ^2S_{1/2}$ atomic line at 5978.93 Å. In the spectrum of Fig. 5, medium intensity atomic Si and many Si^+ lines are also present. In the acquisition of the spectrum of the Fig. 5, a cutoff filter was used to filter the second order intense UV silicon atomic lines. This cutoff filter produces a decrease of the intensity with regard to the spectra of the Figs. 3 and 4. Also, in the recording of the spectra of Figs. 6 and 7, a cutoff filter was used to suppress high diffraction orders. In the LIB emission spectrum observed in the 6180–7620 Å region (Fig. 6), the predominant emitting species are the first line of the Balmer series H_α $n=2 \leftarrow n=3$ at 6562.85 Å and two intense lines of Si^+ corresponding to the transitions $3s^24s\ ^2S_{1/2} \leftarrow 3s^24p\ ^2P^0_{3/2}$ at 5347.10 Å and $3s^24s\ ^2S_{1/2} \leftarrow 3s^24p\ ^2P^0_{1/2}$ at 5371.36 Å. In the spectrum of Fig. 6, several weak atomic lines of Si and Si^+ are also present. The last part of the LIB spectrum corresponding to the 7600–8790 Å region (Fig. 7) is characterized by many weak lines of the Si, Si^+, Si^{2+}, and Si^{3+} atomic fragments.

In order to get more insight into LIB of trisilane and to obtain an unambiguous assignment of the emission lines, we have scanned the corresponding wavelength regions with higher resolution (~0.12 Å in first order), which was sufficient to distinguish clearly between nearly all observed lines.

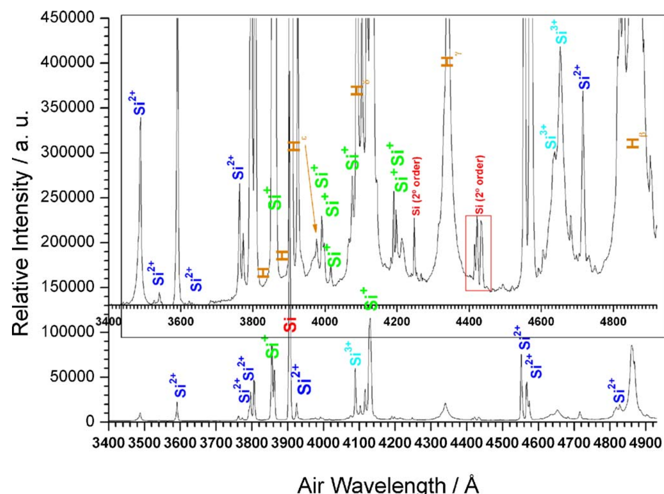

FIG. 4. (Color online) Low-resolution LIB emission spectrum observed in the 3400–4910 Å region in trisilane.

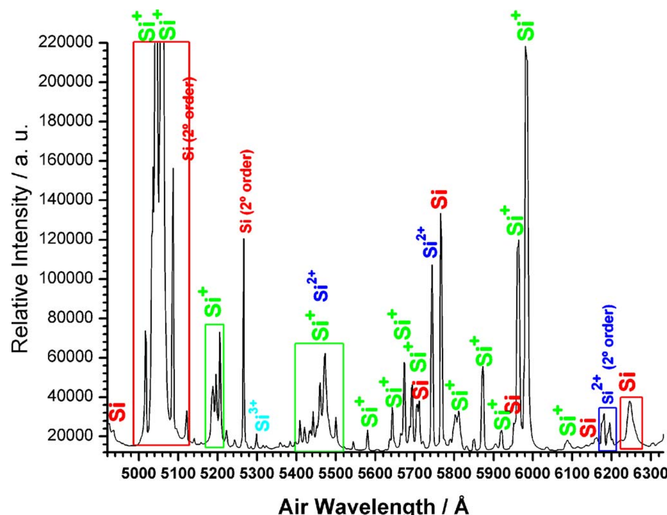

FIG. 5. (Color online) Low-resolution LIB emission spectrum observed in the 4920–6320 Å region in trisilane.

Downloaded 22 Jan 2013 to 161.111.22.141. Redistribution subject to AIP license or copyright; see http://jap.aip.org/about/rights_and_permissions

FIG. 6. (Color online) Low-resolution LIB emission spectrum observed in the 6180–7620 Å region in trisilane.

FIG. 8. (Color online) High-resolution LIB emission spectrum observed in the 2055–2360 Å region in trisilane gas at a pressure of 650 Pa, excited by the 10P(20) line at 944.20 cm^{-1} of the CO_2 laser, and assignment of some atomic lines of Si, Si^{+}, and Si^{2+}.

The spectra have been obtained with 24 successive exposures on the CCD camera in the spectral region 2000–7500 Å by a ISA Jobin Yvon Spex 0.32 m spectrometer. As examples, Figs. 8–14 show several spectra recorded in the LIB experiment. These LIB emission spectra were recorded under the same experimental conditions as low-resolution spectra [pressure 650±5 Pa, excitation line 10P(20) at 10.591 μm of the CO_2 laser and laser power density of 0.86 GW cm^{-2}]. Figures 8–14 display the details of the large features found in Figs. 3 and 4. No new features were observed in these high-resolution spectra. In these figures, multiplet transitions between different J levels for Si, Si^{+}, Si^{2+}, and Si^{3+} are shown. In some cases these multiplet structures are not completely resolved due to Stark broadening of atomic lines. The relative intensities of the observed emission lines reasonably agree with tabulated values in NIST Atomic Spectral Database.[37] The spectral features clearly show the complexity of the relaxation process and bring out the possibility of cascading processes.

C. Plasma temperature measurements

The excitation temperature T_{exc} was calculated according to the Boltzmann equation under the assumption of LTE. The significance of this temperature depends on the degree of equilibrium within the plasma. For an optically thin plasma, the conditions satisfying this assumption of LTE require that the radiative population rates are negligible compared to the collisional population rates. This essentially implies that an excited state must have a higher probability of de-excitation by collision than by spontaneous emission. For a plasma in LTE, any point can be described by its local values of temperature, density, and chemical composition. However, in many cases, the conditions for LTE are not found. In a non-LTE plasma all equilibrating collisional processes are not significantly faster than other plasma processes. Generally, LTE is established among all the species in the plasma beyond ~1 μs delay time from the plasma start. Initially, the excitation temperature was calculated from the relative inten-

FIG. 7. (Color online) Low-resolution LIB emission spectrum observed in the 7600–8790 Å region in trisilane.

FIG. 9. (Color online) High-resolution LIB emission spectrum observed in the 2350–2645 Å region in trisilane.

Downloaded 22 Jan 2013 to 161.111.22.141. Redistribution subject to AIP license or copyright; see http://jap.aip.org/about/rights_and_permissions

FIG. 10. (Color online) High-resolution LIB emission spectrum observed in the 2350–2645 Å region in trisilane.

sities of some Si^+ atomic lines (4920–6320 Å spectral region) from the slope of the Bolztmann plot $\ln[I_{ki}\lambda_{ki}/g_k A_{ki}]$ versus E_k/k_B (Fig. 15),

$$\ln\left[\frac{I_{ki}\lambda_{ki}}{g_k A_{ki}}\right] = C - \frac{E_k}{k_B T_{\mathrm{exc}}}, \qquad (1)$$

where I_{ki} is the emissivity (W m^{-3} sr^{-1}) of the emitted $k \rightarrow i$ spectral line, λ_{ki} is the wavelength, $g_k = 2J_k + 1$ is the statistical weight, A_{ki} is the Einstein transition probability of spontaneous emission, E_k/k_B is the normalized energy of the upper electronic level (k_B is the Boltzmann's constant), and $C = \ln(hcN_k/4\pi Q(T))$ [$Q(T)$ is the partition function]. The values of the λ_{ki}, g_k, A_{ki}, and E_k for Si^+ selected atomic lines were obtained from the NIST Atomic Spectral Database. The estimated excitation temperature was $T_{\mathrm{exc}} = 26000 \pm 3000$ K (Fig. 15). This value is too high for an expanding plasma at a distance of about 100 mm from the central zone of the cell. The same situation was found at radial positions up to 150 mm from the center of the core plasma. In Fig. 15, a great dispersion of data is observed and the estimated excitation temperature is clearly not satisfactory. If the excitation temperature is determined using only the relative intensities of the five first H atomic lines of Balmer series a value of $T_{\mathrm{exc}} = 5600 \pm 300$ K is obtained (Fig. 16). These spectral lines were chosen based on their relative strengths, accuracies, and transition probabilities as listed by the NIST-Atomic Database (2006). The transition probabilities A_{ki}, upper E_k and lower E_i state energies, and statistical weight factors g_k and g_i for the H transitions have been listed in Table I. For transitions in hydrogen $g_\alpha = 2 \times (n_\alpha)^2$, where n_α is the principal quantum number of the electron shell. The excitation temperature determined by using H atomic lines of Balmer series (Table I) was chosen as the first approximation for the excitation temperature. Real plasmas provide, even in the worst cases, just an approximation to LTE. However, their spatial inhomogeneity is very large concerning temperature and number density distributions of the different species. Consequently, the LTE occurs only within a very small volume of the plasma.

FIG. 11. (Color online) High-resolution LIB emission spectrum observed in the 2895–3175 Å region in trisilane.

FIG. 12. (Color online) High-resolution LIB emission spectrum observed in the 3145–3425 Å region in trisilane.

FIG. 13. (Color online) High-resolution LIB emission spectrum observed in the 3700–3940 Å region in trisilane.

Downloaded 22 Jan 2013 to 161.111.22.141. Redistribution subject to AIP license or copyright; see http://jap.aip.org/about/rights_and_permissions

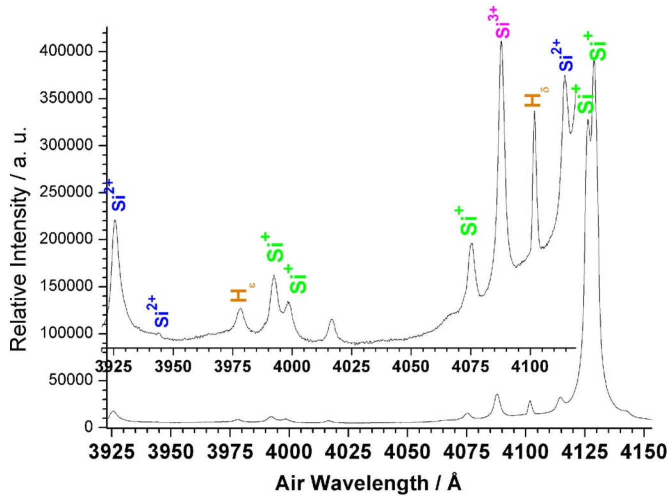

FIG. 14. (Color online) High-resolution LIB emission spectrum observed in the 3920–4155 Å region in trisilane.

D. Ionization degree of the plasma

When LIB is produced in trisilane under high intensity laser radiation, many molecules obtain an energy that exceeds the binding energy. As a consequence, the molecules will dissociate into H and Si atoms and ultimately some atoms can ionize and free or quasifree electrons appear in the laser focal volume. In these conditions Si_3H_8 becomes a mixture of negative electrons, positive ions such as Si^+, Si^{2+}, and Si^{3+}, and H and Si neutral atoms. A gas which contains so many charged particles responsible for its behavior is called plasma. In plasma there is a continuous transition from gases with neutral atoms to plasmas with ionized atoms, which is determined by a dissociation equation. The transition between a gas and a plasma is essentially a chemical equilibrium, which shifts from the gas to the plasma side with increasing temperature. Let us consider the first three different ionization equilibria of silicon,

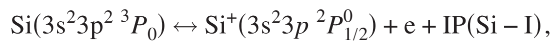

$$\mathrm{Si}(3s^23p^2\ ^3P_0) \leftrightarrow \mathrm{Si}^+(3s^23p\ ^2P^0_{1/2}) + \mathrm{e} + \mathrm{IP(Si-I)},$$

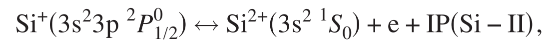

$$\mathrm{Si}^+(3s^23p\ ^2P^0_{1/2}) \leftrightarrow \mathrm{Si}^{2+}(3s^2\ ^1S_0) + \mathrm{e} + \mathrm{IP(Si-II)},$$

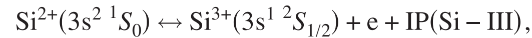

$$\mathrm{Si}^{2+}(3s^2\ ^1S_0) \leftrightarrow \mathrm{Si}^{3+}(3s^1\ ^2S_{1/2}) + \mathrm{e} + \mathrm{IP(Si-III)},$$

where the first three ionization potentials (IPs) for silicon are $E_i^{\mathrm{Si-I}} = \mathrm{IP(Si-I)} = 8.151\,68$ eV, $E_i^{\mathrm{Si-II}} = \mathrm{IP(Si-II)} = 16.345\,84$ eV, and $E_i^{\mathrm{Si-III}} = \mathrm{IP(Si-III)} = 33.493\,00$ eV.[45] For each ionization equilibrium, the LTE between ionization and recombination reactions at temperature T is described by the Saha equation,

$$\frac{N_e N_i}{N_0} = \frac{g_e g_i}{g_0} \frac{(2\pi m_e k_B T)^{3/2}}{h^3} e^{-E_i/k_B T}, \tag{2}$$

where $N_e = N_i$ are the electron and ion densities in the different ionization equilibria in the second member of ionization equilibria, N_0 the density of the silicon or ions in the first member of ionization equilibria, h Planck's constant, k_B Boltzmann's constant, m_e the electron mass, and g_e, g_i, and g_0 the statistical weights of the electrons ($g_e = 2$), Si^+ ions ($g_i = 2$), Si^{2+} ions ($g_i = 1$), Si^{3+} ions ($g_i = 2$), and Si neutrals ($g_0 = 1$). For silicon, the Saha equations read

$$\frac{N_e N_i}{N_0} = C T^{3/2} e^{-E_i/k_B T}, \tag{3}$$

being $C = 9.6587 \times 10^{21}$, 2.4147×10^{21}, and $9.6587 \times 10^{21}\ \mathrm{K}^{-3/2}\ \mathrm{m}^{-3}$ for the first three ionization equilibria of silicon, respectively, and T is in Kelvins. Figure 17 shows the ionization degree $N_i(N_0 + N_i)$ of Si, Si^+, and Si^{2+}, plotted as a function of the gas temperature T, at a constant total pressure $P = (N_0 + N_e + N_i) k_B T$ of 650 Pa. The graph shows that silicon is already fully ionized at thermal energies well below the first ionization energy of 8.151 68 eV (equivalent to 94 596.2 K). At about 1/10 of the ionization energy, the majority of the silicon atoms are ionized (ionization degree of 0.99). Yet, at lower temperatures the electrically charged components of a partially ionized silicon gas may dominate the behavior of the gas.

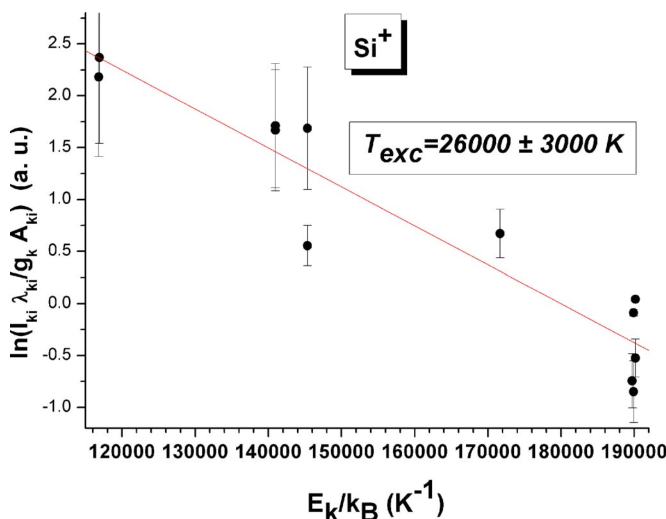

FIG. 15. (Color online) Linear Boltzmann plot for several Si^+ transition lines used to calculate plasma temperature T_{exc}. Plot also shows linear fit to the data with a regression coefficient of $R^2 \sim 0.944$.

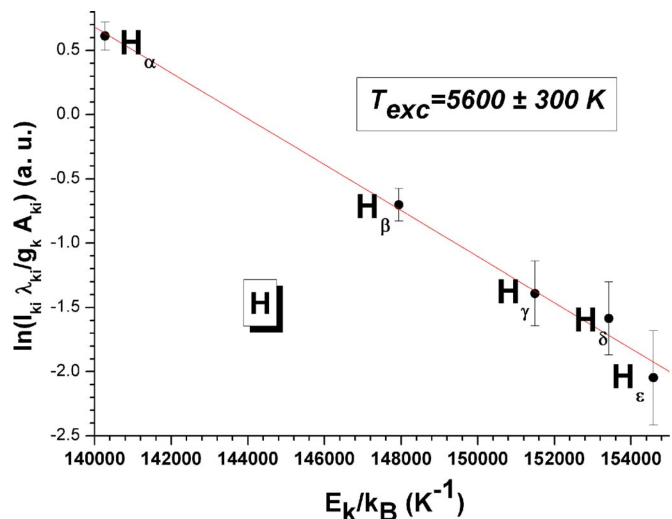

FIG. 16. (Color online) Linear Boltzmann plot for several H transition lines used to calculate plasma temperature T_{exc}. Plot also shows linear fit to the data with a regression coefficient of $R^2 \sim 0.996$.

Downloaded 22 Jan 2013 to 161.111.22.141. Redistribution subject to AIP license or copyright; see http://jap.aip.org/about/rights_and_permissions

TABLE I. List of hydrogen transition lines and their spectral database (NIST Atomic Spectra Database, 2006) used for plasma temperature calculation.

Transition $n_1 - n_2$	Customary name	Air wavelength (Å)	g_i	g_k	A_{ki} (s^{-1})	E_i (cm^{-1})	E_k (cm^{-1})	Rel. int./arb. uni.
2–3	H_α	6562.85	8	18	64650000	82259.28	97492.36	327300
2–4	H_β	4861.33	8	32	20620000	82259.28	102823.91	67200
2–5	H_γ	4340.47	8	50	9425000	82259.11	105291.66	27000
2–6	H_δ	4101.74	8	72	5145000	82259.29	106632.17	18500
2–7	H_ε	3970.07	8	98	438900	82259.28	107440.62	1400

E. Electron number density

The evolution of the laser plasma can be divided into several transient phases. The initial plasma (~0–100 ns) is characterized by high electron and ion densities (10^{16}–10^{20} cm^{-3}) and temperatures around 20 000 K. The emission spectrum for the early stage of the plasma is characterized by a continuum background emission due mainly to bremsstrahlung and recombination processes of electrons with ion in the plasma. Emission lines from Si^+, Si^{2+}, and Si^{3+} ions and H and Si atoms can be found after about 300 ns delay. These lines are superimposed on the continuum background. Observed spectral lines are always broadened, partly due to the finite resolution of the spectrometer and partly to intrinsic physical causes.[48] The principal physical causes of spectral line broadening are the Doppler and Stark broadenings. For a Maxwellian velocity distribution and Gaussian line shape the FWHM can be written as, in Å,

$$\Delta\lambda_{1/2}^{D} = 7.16 \times 10^{-7} \lambda \sqrt{T/M}, \quad (4)$$

where T is the temperature of the emitters in kelving and M the atomic mass in atomic mass units. The Doppler linewidths for the four first lines of the Balmer series for different temperatures are shown in Fig. 18. Owing to the high electron densities, the emission lines are mainly broadened by Stark effect. Both ions and electrons produce Stark broadening, but electrons are responsible for the major part because of their higher relative velocities. Stark broadening produces Lorentzian line shapes, except at the line center, where electrostatic interactions with ions cause a dip. The functional dependency of the electron number density on the FWHM for hydrogen lines can be simplified[49] as

$$\Delta\lambda_{1/2}^{S,\mathrm{H}} = 2.50 \times 10^{-9} \alpha_{1/2} N_e^{2/3}, \quad (5)$$

where N_e is the electron density in cm^{-3}. The half-width $\alpha_{1/2}$ parameter for the H_β line is widely used for plasma diagnostic, and it is tabulated for typical temperatures and electron densities.[50] The electron density in the LIB plasma was determined by measuring the Stark broadening of the Balmer-β spectral line.[51] The simple relation between the electron density N_e in cm^{-3} and the Stark broadening of the Balmer-β spectral line, for electron temperature in the range of 1–4 eV ($1\ \mathrm{eV}/k_B = 1.160\,450\,5(20) \times 10^4$ K) and electron density between 10^{14} and 10^{18} cm^{-3}, is

$$N_e = 1.09 \times 10^{16} [\Delta\lambda_{1/2}^{S}(\mathrm{H}_\beta)]^{1.458}, \quad (6)$$

where $\Delta\lambda_{1/2}^{S}(\mathrm{H}_\beta)$ is expressed in nanometers. The resulting value of the FWHM of the Lorentzian profile $\Delta\lambda_{1/2}^{S}(\mathrm{H}_\beta) = 1.62$ nm, with appropriate corrections for other possible broadening mechanisms, yields the value of electron density $N_e = 1.44 \times 10^{16}$ cm^{-3}. Stark widths of isolated silicon spectral lines have been reported in the literature.[52–55] Electron densities in the range of $(0.8–4.5) \times 10^{16}$ cm^{-3} with an esti-

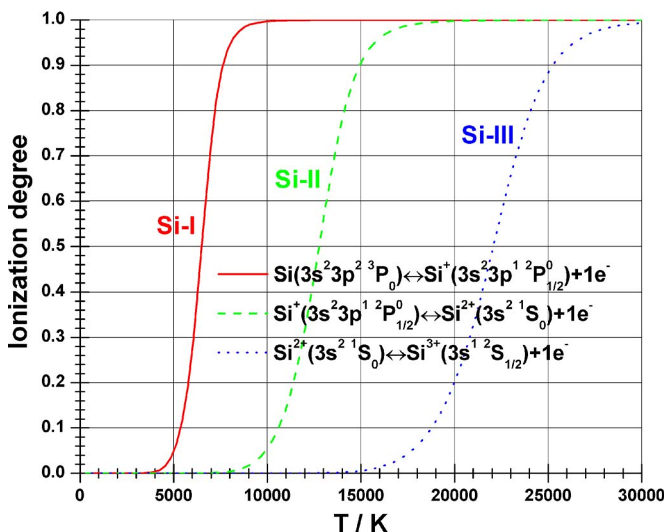

FIG. 17. (Color online) Temperature dependence of the ionization degree $N_i/(N_0+N_i)$ of silicon (Si-I), silicon singly ionized (Si-II), and silicon doubly ionized (Si-III) at a constant pressure of 650 Pa.

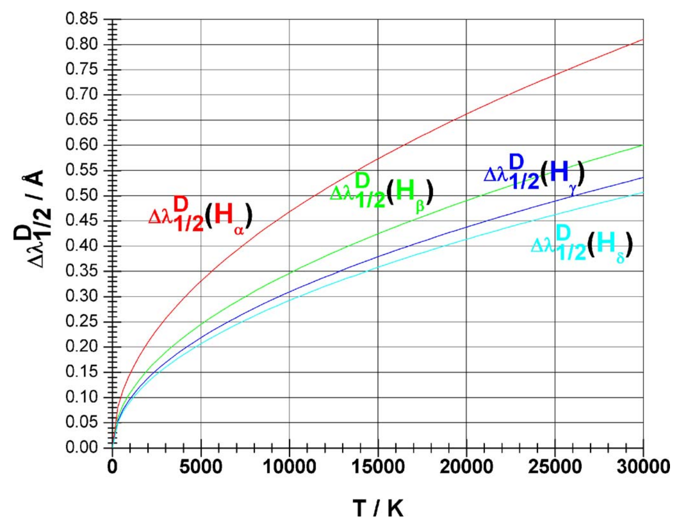

FIG. 18. (Color online) Doppler linewidths for some lines of the hydrogen Balmer series.

Downloaded 22 Jan 2013 to 161.111.22.141. Redistribution subject to AIP license or copyright; see http://jap.aip.org/about/rights_and_permissions

mated uncertainty of 10% were determined from the Stark broadening data of several silicon lines.

F. Laser-induced breakdown mechanism in trisilane

The readily available high-power density of lasers leads to significantly new routes to highly excited states of matter.[56,57] At intensities where the electric field E of the laser radiation approaches and exceeds the nuclear Coulombic potential, the field-induced ionization of atoms via tunneling[58] or complete Coulomb barrier suppression[59] occurs. It is well documented that for the creation of laser-induced plasma various mechanisms may act simultaneously, and that their relative contributions not only depend on initial conditions, but they also change as the plasma grows. The two most important processes involving the formation of a laser-induced plasma are the multiphoton ionization and the formation of an electron cascade or inverse bresmsstrahlung. While the multiphoton ionization process is self-sufficient, the electron cascade requires the presence of at least one electron in the laser focal region. The multiphoton ionization process involves the simultaneous absorption of a number of photons required to equal the ionization potential of a gas. Obviously, for CO_2 laser radiation $h\nu = 0.177063$ eV and the ionization potential of silicon is 8.152 eV, and therefore the photoelectric effect is not possible. However, a multiphoton ionization process is possible, in which an atomic electron is released as the result of the simultaneous absorption of 70 photons. In general, the probability w_n of an atom absorbing simultaneously n photons in the field E corresponding to a photon flux density F is $w_n \propto F^n \propto E^{2n}$. E is the root-mean-square electric field, i.e., the amplitude of the field oscillations $E = \sqrt{2}E_0$ and $F = J(\text{power density in W cm}^{-2})/h\nu$ (in photons $\text{cm}^{-2}\,\text{s}^{-1}$). As it can be seen, the dependence on the laser field is very sharp. Bebb and Gold[60–62] concluded that although multiphoton ionization may supply the initial electrons, it does not account entirely for the breakdown phenomenon, except possibly at very low pressures when the formation of an electron cascade is inhibited. Moreover, it has been established[60–62] that the threshold photon flux density F_{th} or, equivalently, the threshold power density J_{th} for multiphoton ionization varies with $P^{-1/n}$, where P is the gas pressure and n is the number of simultaneously absorbed photons. Therefore, multiphoton ionization predicts a very weak dependence of J_{th} on P for trisilane. However, as we can see from Fig. 2, the breakdown threshold power density in trisilane versus pressure shows a minimum around 400 Pa. The electron cascade process is the absorption of light photon by free or quasifree electrons ($e + h\nu \rightarrow e^*$). The free or quasifree electrons can be produced by multiphoton ionization of any atomic or molecular species including impurities of trisilane (SiH_4, Si_2H_6, N_2, O_2, Ar, etc.) or by natural ionization due to cosmic radiation. These electrons gain sufficient energy to ionize any particle (atom, molecule or ion) by inelastic electron-particle collision, resulting in two electrons of lower energy being available to start the process again. The ionization processes can be described in a general way as

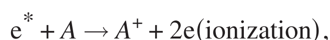

$$e^* + A \rightarrow A^+ + 2e(\text{ionization}),$$

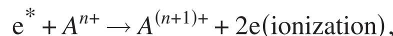

$$e^* + A^{n+} \rightarrow A^{(n+1)+} + 2e(\text{ionization}),$$

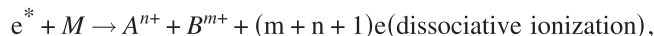

$$e^* + M \rightarrow A^{n+} + B^{m+} + (m + n + 1)e(\text{dissociative ionization}),$$

where A and B refer to atomic or ionic species and M refers to molecular species. Molecular species that can be involved in these processes can be SiH, SiH_3, Si_2, etc. As we have pointed out above, these molecular species can exist, but they have not been spectroscopically detected and therefore we think that the processes of dissociative ionization have minor importance in our experiment than the ionization processes. Breakdown will occur if the electron density can reach a critical value despite the losses due to diffusion. In sufficiently strong fields, it is only necessary for the electrons to excite different species, which are then rapidly ionized by the absorption of a few photons. However, if the laser field is not strong enough to provide rapid ionization of the excited species (atoms, molecules, or ions), the energy lost by the electrons during the excitation hinders the development of the cascade. Figure 2 shows the variation of the threshold power density versus the pressure of trisilane. Note that in all experiments reported here the threshold power density is determined either by observing the appearance of the bright flash of light in the laser focal region visually, detecting also the spectrum or by observing the abrupt absorption of the CO_2 laser pulse that has been transmitted through the focal region. It can be seen that the pressure dependence is incompatible with multiphoton ionization which predicts a very weak $P^{-1/n}$ dependence for the threshold power density, while it is in qualitative agreement with an electron cascade. A minimum in the variation of the threshold power density versus pressure is predicted by the classical theory.[63,64] In our experiments, a minimum in the threshold power density versus pressure curve (Fig. 2) is observed. This fact allows us to conclude that, although the first electrons must appear via multiphoton ionization, electron cascade is the main mechanism responsible for the breakdown in trisilane.

IV. CONCLUSIONS

Laser-induced breakdown generated by CO_2 laser pulses in trisilane gas has been investigated by means of OES. The plasma produced in Si_3H_8 with pressures ranging from 50 to 1000 Pa has been measured and analyzed. Optical breakdown threshold intensities in trisilane at 10.591 μm have been measured. The strong emission observed in the plasma region is mainly due to the relaxation of excited atomic H and Si and ionic fragments Si^+, Si^{2+}, and Si^{3+}. An excitation temperature around 5600 K was calculated by means of hydrogen atomic lines assuming LTE. Electron densities around $1.44 \times 10^{16}\ \text{cm}^{-3}$ can be estimated from the Stark-broadened H_β line shape with appropriate corrections for other broadening mechanisms. The physical processes leading to LIB of trisilane in the power density range $0.28\ \text{GW cm}^{-2} < J < 3.99\ \text{GW cm}^{-2}$ have been analyzed. On the basis of our observations, we propose that, although the first electrons must appear via multiphoton ionization of any molecular species present in the focal volume or by natural ionization, electron cascade is the main mechanism responsible for the breakdown in trisilane.

Downloaded 22 Jan 2013 to 161.111.22.141. Redistribution subject to AIP license or copyright; see http://jap.aip.org/about/rights_and_permissions

ACKNOWLEDGMENTS

This work was partially supported by the Spanish MEC Project No. CTQ2007-60177/BQU. It is a pleasure to acknowledge the excellent technical support of A. Magro. This work is dedicated in memory of Professor Antonio Pardo Martinez.

[1]Y. R. Shen, *The Principles of Nonlinear Optics* (Wiley, New York, 1984).
[2]G. M. Weyl, in *Laser Induced Plasma and Application*, edited by L. J. Radziemski and D. A. Cremers (Dekker, New York, 1989).
[3]H. Takagi, H. Ogawa, Y. Yamazaki, A. Ishizaki, and T. Nakagiri, Appl. Phys. Lett. **56**, 2379 (1990).
[4]Y. Kanemitsu, T. Ogawa, K. Shiraishi, and K. Takeda, Phys. Rev. B **48**, 4883 (1993).
[5]Y. Yamada, T. Orii, I. Umezu, Sh. Takeyama, and T. Yoshida, Jpn. J. Appl. Phys., Part 1 **35**, 1361 (1996).
[6]A. V. Kabashin, J.-P. Sylvestre, S. Patskovsky, and M. Meunier, J. Appl. Phys. **91**, 3248 (2002).
[7]K. M. A. El-Kader, J. Oswald, J. Koka, and V. Chab, Appl. Phys. Lett. **64**, 2555 (1994).
[8]R. E. Hummel, A. Morrone, M. Ludwig, and S.-S. Chang, Appl. Phys. Lett. **63**, 2771 (1993).
[9]E. Edelberg, S. Bergh, R. Naone, M. Hall, and B. S. Aydil, Appl. Phys. Lett. **68**, 1415 (1996).
[10]G. J. Meeusen, E. A. Ershov-Pavlov, R. F. G. Meulenbroeks, M. C. M. van de Sanden, and D. C. Schram, J. Appl. Phys. **71**, 4156 (1992).
[11]T. Glenewinkel-Meyer, J. A. Bartz, G. M. Thorson, and F. F. Crim, J. Chem. Phys. **99**, 5944 (1993).
[12]W. M. M. Kessels, J. P. M. Hoefnagels, M. G. H. Boogaarts, D. C. Schram, and M. C. M. van de Sanden, J. Appl. Phys. **89**, 2065 (2001).
[13]H. Umemoto, K. Ohara, D. Morita, Y. Nozaki, A. Masuda, and H. Matsumara, J. Appl. Phys. **91**, 1650 (2002).
[14]M. Santos, L. Diaz, M. Urbanova, Z. Bastl, J. Subrt, and J. Pola, J. Photochem. Photobiol., A **188**, 399 (2007).
[15]H. Kanoh, O. Sugiura, and M. Matsumura, Jpn. J. Appl. Phys., Part 1 **32**, 2613 (1993).
[16]B. A. Scott, M. H. Brodsky, D. C. Green, P. B. Kirby, R. M. Plecenik, and E. E. Simonyi, Appl. Phys. Lett. **37**, 725 (1980).
[17]*Principles of Laser Plasma*, edited by G. Bekefi (Wiley, New York, 1976).
[18]*Laser lnduced Plasma and Applications*, edited by L. J. Radzienxki and D. A. Cremers (Dekker, New York, 1989).
[19]V. Majidi and M. R. Joseph, Crit. Rev. Anal. Chem. **23**, 143 (1992).
[20]F.-Y. Yueh, J. P. Singh, and H. Zhang, *Laser-lnduced Breakdown Spectroscopy, Elemental Analysis*, Encyclopedia of Analytical Chemistry, edited by R. A. Meyers (Wiley, Chichester, 2000).
[21]D. A. Cremers and L. J. Radziemski, *Handbook of Laser-lnduced Breakdown Spectroscopy* (Wiley, Chichester, 2006).
[22]*Laser-lnduced Breakdown Spectroscopy*, edited by A. W. Miziolek, V. Palleschi, and I. Schechter (Cambridge University Press, Cambridge, England, 2006).
[23]M. D'Orazio and B. Schrader, J. Raman Spectrosc. **2**, 585 (1974).
[24]J. Reader, C. J. Sansonetti, and J. M. Bridges, Appl. Opt. **35**, 78 (1996).
[25]C. H. Chan, C. D. Moody, and W. B. McKnight, J. Appl. Phys. **44**, 1179 (1973).
[26]C. H. Chan and C. D. Moody, J. Appl. Phys. **45**, 1105 (1974).
[27]Y. E. E.-D. Gamal, N. M. Abdel-Monelm, J. Phys. D **20**, 757 (1987).
[28]N. Kroll and K. M. Watson, Phys. Rev. A **5**, 1883 (1972).
[29]Y. E. E.-D. Gamal and I. M. Azzouz, J. Phys. D **34**, 3243 (2001).
[30]D. C. Smith, Appl. Phys. Lett. **19**, 405 (1971).
[31]D. I. Rosen and G. Weyl, J. Phys. D **20**, 1264 (1987).
[32]J. Striker and J. G. Parker, J. Appl. Phys. **53**, 851 (1982).
[33]T. Gasmi, H. A. Zeaiter, G. Ropero, and A. González-Ureña, Appl. Phys. B: Lasers Opt. **71**, 169 (2000).
[34]R. Becerra, M. Ponz, M. Castillejo, M. Oujja, J. Ruiz, and M. Martin, J. Photochem. Photobiol., A **101**, 1 (1996).
[35]G. S. Fu, W. Yu, X. W. Li, L. Han, and L. S. Zhang, Phys. Rev. E **52**, 5304 (1995).
[36]Y. Nozaki, M. Kitazoe, K. Horii, H. Umemoto, A. Masuda, and H. Matsumura, Thin Solid Films **395**, 47 (2001).
[37]NIST Atomic Spectra Database online at http://physics.nist.gov/PhysRefData/ASD/index.html
[38]A. Fowler, Proc. R. Soc. London, Ser. A **123**, 422 (1929).
[39]A. G. Shenstone, Proc. R. Soc. London, Ser. A **261**, 153 (1961).
[40]W. L. Wiese, M. W. Smith, and B. M. Glennon, Natl. Stand. Ref. Data Ser. (U.S., Natl. Bur. Stand.) **4**, 1 (1966).
[41]C. E. Moore, Natl. Stand. Ref. Data Ser. (U.S., Natl. Bur. Stand.) **3**, 15 (1967).
[42]V. Kaufman and B. Edlén, J. Phys. Chem. Ref. Data **3**, 825 (1974).
[43]C. E. Moore, C. M. Brown, G. D. Sandlin, S. G. Tilford, and R. Tousey, Astrophys. J., Suppl. **33**, 393 (1977).
[44]J. Reader, C. H. Corliss, W. L. Wiese, and G. A. Martin, NBS Spec. Publ. **68** (1980).
[45]W. C. Martin and R. Zalubas, J. Phys. Chem. Ref. Data **12**, 323 (1983).
[46]F. Blanco, B. Botho, and J. Campos, Phys. Scr. **52**, 628 (1995).
[47]J. R. Fuhr and W. L. Wiese, *NIST Atomic Transition Probability Tables*, CRC Handbook of Chemistry and Physics, 77th ed., edited by D. R. Lide (CRC, Boca Raton, FL, 1996).
[48]*Atomic, Molecular and Optical Physics Handbook*, edited by G. W. F. Drake (AIP, Woodbury, New York, 1996).
[49]W. L. Wiese, in *Plasma Diagnostic Techniques*, edited by R. H. Huddlestone and S. C. Leonard (Academic, New York, 1965).
[50]*Astrophysical Quantities*, edited by A. N. Cox (AIP, New York, 1996).
[51]J. Torres, J. Jonkers, M. J. van de Sande, J. J. A. M. van der Mullen, A. Gamero, and A. Sola, J. Phys. D **36**, 55 (2003).
[52]J. Meyer and R. J. Beck, Astron. Astrophys. **8**, 93 (1970).
[53]M. H. Miller and R. D. Bengtson, Phys. Rev. A **1**, 983 (1970).
[54]J. Puric, S. Djenize, J. Labat, and L. J. Cirkovic, Z. Phys. **267**, 71 (1974).
[55]N. Konjevic and J. R. Roberts, J. Phys. Chem. Ref. Data **5**, 209 (1976).
[56]M. D. Perry and G. Mourou, Science **264**, 917 (1994).
[57]P. B. Corkum, M. Y. Ivanov, and J. S. Wright, Annu. Rev. Phys. Chem. **48**, 387 (1997).
[58]L. V. Keldysh, Sov. Phys. JETP **20**, 137 (1965).
[59]S. Augst, D. D. Strickland, and S. L. Chin, J. Opt. Soc. Am. B **8**, 858 (1991).
[60]H. B. Bebb and A. Gold, *Multiphoton Ionization of Hydrogen and Rare Gas Atoms*, Physics of Quantum Electtronics, edited by P. L. Kelly, B. Lax, and P. E. Tannenwald (McGraw-Hill, New York, 1966).
[61]H. B. Bebb and A. Gold, Phys. Rev. **143**, 1 (1966).
[62]A. Gold and H. B. Bebb, Phys. Rev. Lett. **14**, 60 (1965).
[63]Y. B. Zel'dovich and Y. P. Raiser, Sov. Phys. JETP **21**, 190 (1965).
[64]C. Demichelis, IEEE J. Quantum Electron. **5**, 188 (1969).

Downloaded 22 Jan 2013 to 161.111.22.141. Redistribution subject to AIP license or copyright; see http://jap.aip.org/about/rights_and_permissions